Published in final edited form as:
Free Radic Biol Med. 2010 April 15; 48(8): 1034–1043. doi:10.1016/j.freeradbiomed.2010.01.020.

Early and late administration of MnTE-2-PyP^{5+} in mitigation and treatment of radiation-induced lung damage

Benjamin Gauter-Fleckenstein, M.D.[1,2], **Katharina Fleckenstein, M.D.**[1,3], **Kouros Owzar, Ph.D.**[4,5], **Chen Jiang, Ph.D.**[5], **Reboucas Julio, Ph.D.**[1], **Ines Batinic-Haberle, Ph.D.**[1], and **Zeljko Vujaskovic, M.D., Ph.D.**[1]

[1]Department of Radiation Oncology, Duke University Medical Center, Durham, NC 27710

[2]Department for Anesthesiology and Intensive Care Medicine, Mannheim Medical Center, Heidelberg University, Mannheim, Germany

[3]Department of Radiation Oncology, Mannheim Medical Center, Heidelberg University, Mannheim, Germany

[4]Department of Biostatistics and Bioinformatics, Duke University Medical Center, Durham, NC 27710

[5]Biostatistics and Computational Biology Core, RadCCORE, Duke University Medical Center

Abstract

Introduction—Chronic production of reactive oxygen and nitrogen species is an underlying mechanism of radiation (IR)-induced lung injury. The purpose of this study was to determine the optimum time of an antioxidant and redox-modulating Mn porphyrin, MnTE-2-PyP^{5+}, delivery to mitigate and/or treat IR-induced lung damage.

Methods—Female Fischer-344 rats were irradiated to their right hemithorax (28 Gy). Irradiated animals were treated with PBS or MnTE-2-PyP^{5+} (6 mg/kg/24h) delivered for 2 weeks by s.c.-implanted osmotic pumps (beginning after 2, 6, 12, 24, 72 hours or 8 weeks). Animals were sacrificed 10 weeks post IR. Endpoints were: body weight, breathing frequency, histopathology, and immunohistochemistry (8-OHdG; ED-1; TGF-β; HIF-1α; VEGF [A]).

Results—A significant radioprotective effect on functional injury, measured by breathing frequencies, was observed for all animals treated with MnTE-2-PyP^{5+}. Treatment with MnTE-2-PyP^{5+} starting 2 h, 6 h, and 12 h but not after 24 h or 72 h resulted in a significant decrease in immunostaining for 8-OHdG, HIF-1α, TGF-β, and VEGF (A). A significant decrease in HIF-1α, TGF-β, and VEGF (A), as well as an overall reduction in lung damage (histopathology) was observed in animals beginning treatment at the time of fully developed lung injury (8 weeks post IR).

Conclusion—The catalytic manganese porphyrin antioxidant and modulator of redox-based signalling pathways, MnTE-2-PyP^{5+}, mitigates radiation-induced lung injury when given within

Corresponding Author: Zeljko Vujaskovic, M.D., PhD, DUKE University Medical Center, Department of Radiation Oncology, Durham, NC 27710, Tel: 919 681 1675, Fax: 919 681 2651, vujas@radonc.duke.edu.

The first two authors contributed equally to this manuscript.

the first 12 hours after IR. More importantly, this is the first study to demonstrate MnTE-2-PyP^{5+} can reverse overall lung damage when started at the time of established lung injury 8 weeks post IR. The radioprotective effects are presumably mediated through both its ability to suppress oxidative stress as well as to decrease activation of key transcription factors and proangiogenic and profibrogenic cytokines.

Keywords

radiation; lung injury; oxidative stress; manganese porphyrin; radioprotector; MnTE-2-PyP^{5+}

Introduction

Recent investigations support the notion that radiation-induced lung injury is initiated and sustained by oxidative stress [1, 2]. The initial source of oxidative stress arises from radiolytic hydrolysis of water to produce hydroxyl radical which rapidly reacts with cellular macromolecules to cause DNA, lipid and protein damage. Studies from cell culture irradiation point to both phagocytic/nonphagocytic NADPH oxidase, nitric oxide synthases, and mitochondria as major sources of reactive oxygen/nitrogen species (ROS/RNS), initiating and sustaining a highly oxidized microenvironment [3-6]. This results in a plethora of reactive oxygen and nitrogen species such as carbonate radical ($CO_3^{\bullet -}$), peroxynitrite ($ONOO^-$), hypochlorous acid (HOCl), hydrogen peroxide (H_2O_2), superoxide ($O_2^{\bullet -}$), and hydroxyl radical ($HO^{\bullet}$). At later stages of the inflammation process, recruitment and activation of macrophages contribute to further increasing levels of superoxide and hydrogen peroxide through NADPH oxidase with successive formation of the aforementioned species. Several transcription factors (NF-κB, HIF-1α, AP-1, and SP-1) and subsequently their downstream products (TGF-β, VEGF(A), EGF, and CA IX) are known to be directly or indirectly regulated by oxidative stress; i.e. oxidation, nitration and/or nitrosation events [3, 7-9]. Consequently, compounds which exhibit antioxidant properties have been evaluated as modulators of radiation-induced lung injury [10-17]. The most promising compounds are mimics of superoxide dismutase enzymes (SOD) – a first line enzyme of endogenous antioxidant systems. So far several groups of SOD-mimics have been developed and tested in different models of oxidative stress such as manganese porphyrins (MnPs) [18, 19], manganese (II) penta-azamacrocyclic complexes [20], manganese (III) salen complexes [21], and nitroxides [22]. The in vitro and in vivo effects have been recently reviewed [23]. In addition, other synthetic antioxidants such as MitoQ compounds targeting mitochondria have also been studied [24]. Only few comparative studies have been thus far performed. In an *E. coli* study manganese (II) penta-azamacrocyclic complexes (M40403), and manganese (III) salen complexes (EUK-8 and EUK-134) were ineffective. Only MnTE-2-PyP^{5+} and MnTM-2-PyP^{5+} were able to rescue aerobic growth of SOD-deficient *E. coli* [25]. Another recent study again compared the aforementioned compounds (manganese (II) penta-azamacrocylclic complexes M40403, manganese (III) salen complexes EUK-8 and EUK-134, and 6 MnPs) with $MnCl_2$ as a control. Only the hexyl analogue of MnTE-2-PyP^{5+}, MnTnHex-2-PyP^{5+}, was able to radioprotect ataxia telangiectasia cells [26].

MnPs and manganese (III) salen complexes [27] have been tested as radioprotectors in models of radiation-induced lung damage. In this respect, MnPs have proven to be potent radioprotectors in the rat model of radition-induced lung injury [10-13, 28]. At least in part, the in vivo efficacy of MnPs is due to their localization in mitochondria [29], where MnTE-2-PyP^{5+} was shown to protect the mitochondrial respiratory chain from $ONOO^-$ -mediated damage [30]. The efficacy of most potent SOD mimics in dismuting superoxide parallels their ability to scavenge $ONOO^-$ and its decomposition product $CO_3^{\bullet -}$ [31]. The ability to reduce HClO has been indicated [23]. Furthermore, by scavenging reactive

species, MnPs were shown to inhibit activation of major redox-regulated transcription factors NF-κB, AP-1, and HIF-1α, and expression of their downstream gene targets [8, Zhao et al 2005, 9, 15].

Our recent investigations have focused on preemptive or early (within a few hours following the irradiation insult) administration of MnPs to prevent and ameliorate lung injury after irradiation (IR) [10-13]. In the event of a nuclear accident [32] or deliberate attack resulting in a large population exposure to ionizing radiation, victims will need to be triaged according to the severity of acute radiation illness. Acutely, lung injury is not of paramount importance. However, with successful treatment of gastrointestinal and hematologic syndromes with modern medical advances, mortality from respiratory distress may later become an issue [33]. Furthermore, many victims at risk for development of chronic injury will not be symptomatic for months to years following exposure. Therefore, it is necessary to identify therapeutic compounds, which are effective when delivered after the onset of symptomatic injury.

Although the threat of nuclear terrorism or accident has increased in recent years, the major benefit for normal tissue radioprotectors will be for cancer patients undergoing radiotherapy for tumors in the thoracic region. Up to 20% of these patients will eventually develop radiation (IR)-induced normal lung tissue injury. Furthermore, with respect to lung cancer, several clinical studies have shown a direct relationship between tumor cell killing and increasing radiation dose which points to the importance of dose escalation for achieving improved local control and possible increasing overall survival [34-38]. However, dose escalation and improved tumor control is limited by the unacceptable risk for normal tissue toxicity. At present, no strategy exists which robustly identifies patients who will develop normal tissue injury after IR [39]. Therapeutic interventions which could be delayed until the onset of symptoms may lower cost, preserve drug availability, and eliminate possible side effects of prolonged administration.

The purpose of this study was to investigate the efficacy of our lead compound, MnTE-2-PyP^{5+}, in treating radiation-induced lung injury in our established model, if applied at early (within 72 hours) or late (up to 8 weeks) time points after radiation.

Materials and Methods

Animals

Fifty-four female Fischer-344 (F344) rats were used in this study with prior approval from the Duke University Institutional Animal Care and Use Committee. Three animals were housed per cage and maintained under identical conditions with food and water provided *ad libitum*. All rats were sacrificed at a predetermined time of ten weeks post-radiation by pentobarbital overdose.

Drug

MnTE-2-PyP^{5+} was synthesized and characterized as previously described [40]. The manganese porphyrin used in this study was dissolved in PBS.

Irradiation and Sod Mimetics

At the time of irradiation all rats weighed between 175 and 185 g to minimize possible variations in lung size. The 54 animals were divided equally into the following groups to receive: 1) right hemithoracic irradiation (IR) and PBS starting 2 hours after IR; 2) no IR and MnTE-2-PyP^{5+}; 3) no IR and PBS; 4) IR and MnTE-2-PyP^{5} starting 2 hours after IR; 5) IR and MnTE-2-PyP^{5+} starting 6 hours after IR; 6) IR and MnTE-2-PyP^{5+} starting 12 hours

after IR; 7) IR and MnTE-2-PyP^{5+} starting 24 hours after IR; 8) IR and MnTE-2-PyP^{5+} starting 72 hours after IR; and 9) MnTE-2-PyP^{5+} starting 8 weeks after IR.

Animals were anesthetized before IR with intraperitoneal injection of ketamine (65 mg/kg) and xylazine (4.5 mg/kg) and placed in a prone position. Non-irradiated control animals were kept during the sham-irradiation procedure without anesthesia in a cage near the X-ray machine while mates were irradiated. Hemithoracic radiation was delivered to the right lung with a single dose of 28 Gy using 150 kV x-rays with a dose rate of 0.71 Gy/min (Therapax 320, Pantak Inc., East Haven, CT). 12 mm lead blocks were used to protect the left thorax and the rest of the body. MnTE-2-PyP^{5+} was applied at a dose of 6 mg/kg/24h, the most effective dose determined in previous studies [10]. MnTE-2-PyP^{5+} or PBS were delivered subcutaneously by osmotic pumps (Alzet® Model 2ML2, Durect Corporation, Cupertino, CA) at a dose rate of 5.0 μl/h for 14 days. The total volume per osmotic pump was 2 ml. Drug delivery began at the following time points post-IR: 2, 6, 12, 24, 72 hours, and 8 weeks for the treatment groups and 2h after IR for controls.

Follow-Up and Functional Assessment of Lung Injury

All animals were followed for ten weeks after IR (see time table). Body weight was measured bi-weekly. Breathing frequency using whole-body plethysmography (Model RM-80, Columbus Instruments, Columbus, OH, USA) was measured as an indicator of functional pulmonary injury. Measurements were taken every 2 weeks for 10 weeks, starting 4 weeks after IR. The mean values from five measurements per animal were recorded for 5 animals in each group.

Histology

At the time of sacrifice, the right upper lobes of all animals were obtained for immunohistochemistry and histopathology studies. Animals were euthanized with pentobarbital overdose. Both lungs were infused by tracheal instillation of a solution containing 2% glutaraldehyde and 0.085 M sodium cacodylate buffer for 25 minutes for fixation prior to removal of the lung. After removal, the four lobes of the irradiated right lung were separated and embedded in paraffin. The tissue was then cut into 5 μm thick sections at a microtome and stored on slides.

Histopathology

Five-micrometer thick sections of paraffin-embedded lung tissue were stained with hematoxylin and eosin (H&E) to visualize histopathologic damage to lung structures. Slides were systematically scanned under a microscope using a 10× objective and eight to ten fields containing the highest degree of damage were selected. The extent of radiation-induced damage for each field was graded on a scale from 0 (normal lung) to 8 (total obliteration of the field) as described by Ashcroft et al. [41]. Average scoring below grade 4 (moderate thickening of walls without obvious damage to lung architecture) resulted in the animal placement in the “no damage” group while average scoring above grade 4 (increased fibrosis with definite damage to lung architecture) led to the respective animal placement in the “damage” group.

Immunohistochemistry

Lungs were assessed: (A) for the number of activated macrophages with ED-1 staining; (B) the level of expression of 8-OHdG (8-hydroxy-2′-deoxyguanosine) as a marker for oxidative stress/ DNA damage; (C) levels of TGF-β (transforming growth factor-beta), a profibrogenic cytokine; (D) HIF-1α (hypoxia inducible factor 1α), a pro-angiogenic

transcription factor; and (E) VEGF (A) (vascular endothelial growth factor A), a pro-angiogenic cytokine.

Immunohistochemistry was performed as described by Hsu et al. [42]. Briefly, the tissue sections were deparaffinized and rehydrated with xylene and decreasing alcohol concentrations from 100% to 80%. Endogenous peroxidase activity was blocked with 3% hydrogen peroxide for 15 minutes. The slides were then placed in a citrate buffer (Biogenex, San Ramon, CA) and heated in a microwave for 2 × 5 minutes for antigen retrieval. The tissue sections were rinsed with phosphate-buffered saline and incubated with primary antibodies to activated macrophage marker ED1 (MCA341, 1:100, Serotec, Oxford, UK), 8-OHdG (MOG-020P, 1:1000, JaICA, Shizuoka, Japan), VEGF (A) (Sc-152, 1:100, Santa Cruz Biotechnology Inc., Santa Cruz, CA), active TGF-β1 (Sc-146, 1:200, Santa Cruz Biotechnology Inc., Santa Cruz, CA), and HIF-1α (NB 100-105, 1:100, Novus Biologicals, Littleton, CO) overnight at 4°C. Slides were then washed three times in phosphate-buffered saline for 5 minutes followed by incubation with the appropriate secondary antibody (1:1000, Jackson ImmunoResearch, West Grove, PA) for 30 minutes at room temperature. Again slides were washed three times in phosphate-buffered saline for 5 minutes followed by incubation with ABC-Elite (Vector Laboratories, Burlingame, CA) for 30 minutes at room temperature and developed using DAB working solution (Laboratory Vision, Fremont, CA). Finally, the slides were counterstained with Harris hematoxylin (Fisher Scientific, Pittsburgh, PA) and mounted with coverslips. For negative controls, consecutive tissue sections were processed by the same immunostaining protocols. Primary antibodies were ommitted and processed tissues were incubated with secondary antibodies. No staining due to unspecific antibody binding was seen in negative staining controls.

Image Analysis

For image analysis, tissue sections from the upper right lobe from each animal were examined. Image analysis was carried out as previously described [10-12]. Eight digital images were acquired from each slide using a 20× (VEGF, TGF-β, ED-1) or 40× (HIF-1α, 8-OHDG) objective. Activated macrophage marker ED1, 8-OHdG and HIF-1α staining were quantified by manual counting per image. Results were expressed as the number of positively stained macrophages or percent of 8-OHdG/HIF-1α positive nuclei per digital image (average of eight digital images per animal, average of five to six animals per group).

Active TGF-β and VEGF were analyzed in Adobe Photoshop (Version 9.0.2; Adobe Systems, San Jose, CA). After quantifying the positive expression per image, the total tissue area regardless of expression was quantified. Results represent the average percentage of positive staining as the ratio of positive staining over total tissue area per digital image.

Statistical Analysis

The discrepancies between binomial proportions were tested using Fisher's exact test [43]. The distributions of the biomarkers with respect to drug (or dose) were compared in a pairwise fashion using the exact two-sample Wilcoxon test [44]. For breathing frequencies and body weight, an aggregate measure was computed as the empirical area under the curve. The distributions of these curves were compared in a pairwise fashion using the exact two-sample Wilcoxon test [44]. Time-course trajectories of the treatments were compared within the framework of two-way multiplicative mixed-linear effects model [45]. The R statistical environment [46] was used for all statistical analyses.

Results

All animals tolerated treatment with MnTE-2-PyP^{5+} well. Subcutaneous (s.c.) injections of MnTE-2-PyP^{5+} [10], resulted in decreased mobility, local edema, hyperemia/vasodilation (as seen in snout and ears), and reduced body weight during the injection period. In contrast, the controlled injection rate (5μl/h) by s.c. implanted osmotic pumps did not cause any such negative effects.

Body Weight and Breathing Frequencies

Body weight was measured two weeks prior to IR, on the day of IR, and biweekly starting from week two until week ten, the time point of sacrifice (Table 1). Average body weight over all groups was 181.1 ± 2.2 g on the day of irradiation. The weight of the MnP-filled osmotic pump was substracted from the measured body weight. The unirradiated control groups gained weight throughout the entire process. In contrast, irradiated animals receiving no treatment (IR only group) gained significantly less weight (Table 1). With respect to the entire time course over ten weeks, irradiated animals receiving MnTE-2-PyP^{5+} starting at 2 h, 6 h, 24 h, 72 h, and 8 w after IR did not statistically differ in body weight from the irradiated, untreated animals. Animals receiving MnTE-2-PyP^{5+} 12 h after IR displayed significantly higher body weight in comparison to the IR only-group ($P = 0.031$).

Breathing rates were measured in a representative group ($n = 10$) before IR and in 5 animals per group biweekly starting 4 weeks after IR until 10 weeks post IR (Fig. 1; Table 1). In comparison to unirradiated animals, significantly higher breathing rates were measured in animals receiving no treatment after IR ($P = 0.008$). Animals which were irradiated and received early treatment with MnTE-2-PyP^{5+} after IR displayed significantly lower breathing rates irrespective of different starting points (regarding sensitivity of breathing frequency test, see Gauter-Fleckenstein et al. [10]). Animals in which treatment was delayed until 8 weeks post IR, displayed elevated breathing frequencies until MnTE-2-PyP^{5+} was given. Only five days after initiation of MnTE-2-PyP^{5+} administration, a significant drop in breathing frequencies was noted (implantation of pumps at day 5 of week 7; measurement of breathing frequencies five days later at day 3 of week 8). In this group, in comparison to the IR only group, breathing frequencies continued to be decreased until the end of the experiment ($P = 0.032$).

Histopathology

H&E staining showed no damage in the unirradiated control groups (average scoring grade = 0.29 for PBS only and 0.43 for MnTE-2-PyP^{5+} only (Table 1, Fig. 2 and 3). In comparison, 10 weeks after IR the average damage score for animals in the IR-only group was 5.3 (min 0, max 8). The histopathological damage was composed of severe distortion of lung structure, accumulation of alveolar macrophages, interstitial/alveolar edema, and beginning formation of fibrous masses (Fig. 3).

Animals which received MnTE-2-PyP^{5+} starting 2 hours and 12 hours as well as 8 weeks after IR displayed significantly less histopathological damage in comparison to the IR-only group (Table 1, Rank-sum-Test).

With respect to a (true) treatment or amelioration effect after IR, animals receiving MnTE-2-PyP^{5+} begun 2 hours post IR displayed a trend towards decreased damage of lung structure ($P = 0.06$, Fisher's test). Animals whose treatment started 8 weeks post IR showed no significant damage ($P = 0.0152$, Fisher's test). In this group, the picture seen was composed of thickening of the alveolar wall, interstitial/alveolar edema, and sporadic accumulation of macrophages reflecting a score < 4 on the Ashcroft scale ("*no obvious damage to lung structure*" [41]).

Immunohistochemistry

Activated macrophages stain positive for ED-1. Activation and recruitment of macrophages is a hallmark of radiation-induced lung injury. There were no activated macrophages in unirradiated animals. In all irradiated animals, activated macrophages were seen. However, a significantly smaller number of activated macrophages were seen in animals which received MnTE-2-PyP^{5+} after 12 h and after 8 weeks, respectively (both groups P = 0.0043; Fig. 2 and 3, Table 1).

A footprint of oxidative DNA damage is 8-OHdG [47]. No 8-OHdG was detected in the unirradiated control groups. 10 weeks post IR, in comparison to the control groups, DNA oxidation was seen in animals which received no MnTE-2-PyP^{5+} after IR (P = 0.002). Significantly decreased positive immunostaining for 8-OHdG positive nuclei was seen in animals whose treatment with MnTE-2-PyP^{5+} was started 2h, 6h, 12 h, and 24 h post IR, respectively. Starting treatment with MnTE-2-PyP^{5+} at later time points (3 days and 8 weeks) did not result in decreased 8-OHdG levels (Fig. 2 and 3, Table 1).

Active TGF-β seems to be linked with development of fibrosis after irradiation. No positive immunostaining for TGF-β was observed in unirradiated control animals. In comparison, active TGF-β was significantly elevated in the IR-only group (P = 0.0021). Treatment with MnTE-2-PyP^{5+} resulted in decreased active TGF-β levels. Elevated levels of activated TGF-β were observed only in animals receiving MnTE-2-PyP^{5+} starting 24 hrs after IR (Fig. 2 and 3, Table 1).

No positive staining for the transcription factor HIF-1α was seen in the unirradiated control groups. 10 weeks after IR, animals not receiving treatment displayed highly elevated levels of HIF-1α in comparison to unirradiated controls (P = 0.0021). In animals which received MnTE-2-PyP^{5+} at 2 h, 6 h, 12 h, and 8 weeks post IR, decreased levels of HIF-1α were seen (Fig. 2 and 3, Table 1).

HIF-1α is the transcription factor that regulates pro-angiogenic factor VEGF (A) expression. VEGF (A) promotes angiogenesis and endothelial leakage and has been linked to the development of lung fibrosis. Consequently, no positive staining for VEGF (A) was seen in both unirradiated control groups. Significant positive staining for VEGF (A) could be detected in the IR-only group (P = 0.0021). Significantly decreased VEGF (A) levels were seen in the groups of animals, which received MnTE-2-PyP^{5+} starting after 2 h, 6 h, 72h, and 8 w. Furthermore, in comparison to the IR only-group a trend towards decreased VEGF(A) levels was observed in animals receiving MnTE-2-PyP^{5+} starting 12 h after IR (P = 0.082; Fig. 2 and 3, Table 1).

Discussion

Our study describes the efficacy of MnTE-2-PyP^{5+} to ameliorate and/or treat radiation-induced lung injury in a rodent model if given after the insult. Early treatment with MnTE-2-PyP^{5+} between 2 h to 12 h after irradiation and lasting for two weeks, ameliorated radiation-induced lung damage. Most importantly, delay of treatment for up to 8 weeks after radiation exposure, and at the time of symptomatic injury, was strikingly effective in treating radiation-induced lung injury.

Late radiation damage in most tissues is characterized by loss of parenchymal cells and excessive formation of fibrous tissue. The classical target cell concept describes radiation-induced late tissue injury as a consequence of a critical depletion of clonogenic target cells triggered by radiation-induced double strand breaks leading to mitotic cell death [48]. The prolonged latent period preceding development of late sequelae had been attributed to the

long cell cycle time of target cells. However, this simplistic, linear sequence of interaction of ionizing radiation with a specific target cell is not sufficient to describe the rather complex, dynamic and, particulary, multicellular process in radiation-induced lung damage [39, 49, 50]. It is assumed that within hours after radiation, apoptotic cell death of endothelial vascular cells [51] leads to enhanced vascular permeability, edema, and protein exudation [52, 53]. Our group recently identified the temporal onset of events at the molecular level underlying radiation-induced lung injury in an animal model [1]. In those studies, lung perfusion was significantly decreased within the first 3 days after irradiation. This was followed by a brief period of reperfusion prior to a steady and significant decrease in perfusion beginning at 2 weeks and continuing throughout the follow-up period (20 weeks). Throughout this episode of ischemia and reperfusion (I/R), oxidative stress is generated [54]. Early formation of ROS/RNS can activate transcription factors (NF-κB, HIF-1α, Nrf2, AP-1) and signaling kinase pathways (MAPK, PI3K/Akt, Caspases, Bcl-2) crucial for cell survival [3, 55]. Among the first cytokines detected hours after radiation in lung tissue are TGF-β and TNF-α [56, 57]. Other factors, such as endothelin, connective-tissue growth factor, and angiotensin II are hypothesized to play a role within these processes [1, 58]. Subsequently, a perpetual cascade of cytokines is initiated [59]. Within this environment, ROS/RNS and redox-regulated transcription factors as well as redox-sensitive cytokines provide strong targets for antioxidant therapy and prevention, mitigation, and treatment of radiation-induced lung injury [60, 61]. However, during increasing ischemia and pulmonary vasoconstriction, transportation of MnTE-2-PyP^{5+} to affected areas in the lung could be limited. We therefore assume that the observed efficacy of MnTE-2-PyP^{5+} in the lung throughout the early phase up to 12 hours after IR, but not thereafter (24 h and 72 h), reflects at least partially a distribution problem as seen in the lung perfusion study. In addition, increasingly overwhelming activation of inflammation-mediating transcription and growth factors, cytokines, and signaling cascades could result in a critical, relative shortage of the compound leading to its ineffectiveness.

When early treatment cannot be achieved, the question arises whether delayed treatment after several weeks can ameliorate or even reverse radiation-induced lung injury. In other organ systems, studies with ACE inhibitors in treating experimental radiation nephropathy have shown that a delay of treatment 3 weeks after total body irradiation of rats did not compromise efficacy of prophylaxis [62]. Moreover, renal function was maintained after treatment was stopped. In adolescent rats, treatment was most potent during a critical period between 3.5 and 9.5 weeks after total body irradiation [62]. The therapeutic effect was linked to inhibition of angiotensin II and not to antioxidative properties of the drug. Early studies with ACE inhibitors in treating radiation-induced lung fibrosis indicated effectiveness, but cessation of treatment led to rapid deterioration in lung function [63-66]. Similar, clinical studies with pentoxifylline and vitamin E for treating radiation-induced fibrosis demonstrated that long-term treatment was needed to sustain benefit [67]. Lung tissue contains a rather small stem cell pool and a large compartment of functional cells competent of proliferation [68]. The inflammatory response of the lung consists of both a tissue destructive component and a tissue healing effort with unpredictable outcome [69]. Our data suggest that treatment with MnTE-2-PyP^{5+} during the highly active inflammatory phase can redirect tissue remodeling from destruction and fibrosis into tissue healing and reconstruction. At eight weeks, macrophages are activated and hypoxia can be detected. Furthermore, a significantly elevated level of 8-OHdG reflective of ongoing oxidative stress is already present. In addition, VEGF (A) and TGF-β are significantly elevated [1], which was resolved after treatment with MnTE-2-PyP^{5+}. The picture of lung damage as seen in animals treated with MnTE-2-PyP^{5+} starting 8 weeks after radiation until sacrifice at 10 weeks was remarkably different in several ways in comparison with animals whose treatment was initiated at early time points after IR. Although a significant level of cumulative oxidative damage was present, a significantly decreased number of activated

macrophages were noted. Furthermore, the least histopathological damage comprising increased alveolarwall thickness, rarefication of alveolar wall architecture, and interstitial fluid deposition was seen in the 8 weeks group. These altered lung structures might be residual from prior inflammation and eventual remodeling processes.

A striking finding in this study was decreased breathing frequencies only 5 days after starting MnTE-2-PyP^{5+}-treatment in the 8 weeks group (Figure 1). A major cause of elevated breathing frequencies is systemic hypoxemia or hypercapnia. In normocapnic rats, it has been shown that breathing frequencies depend on hypoxia [70]. In previous studies it was shown that local hypoxia developed in lung tissue after radiation [1]. This was linked to edema, deposition of intercellular matrix material, destruction of the alveolar histoarchitecture and, accumulation of activated macrophages, which heavily consume oxygen by their endogenous enzyme NADPH-oxidase [71, 72]. However, considering the histopathologically focal picture of radiation-induced lung damage, it is unlikely that systemic hypoxia developed in our model since the adjacent healthy lung tissue, as well as the contralateral lung, most likely were able to compensate for local tissue hypoxia. Recently, it was shown that central stimulation of basal ventilation is enhanced by upregulation of activity in carotid artery bodies without detection of hypoxia [73]. It has been suggested that proinflammatory cytokines (IL-1, IL-6) may be responsible for sensitization of oxygen sensing of chemoreceptors as the rat carotid artery body expresses interleukin receptors [74, 75]. In contrast, ROS do not seem to be involved in modulating chemoreceptor activity [76]. MnTE-2-PyP^{5+} obviously decreases IL-1 induced myocardial depression [77] and protects NIT-1 insulinoma cells from IL-1 induced cytotoxicity [78]. Therefore, the observed decrease in breathing frequencies could be an indirect MnTE-2-PyP^{5+}-mediated effect leading to diminished expression of inflammatory cytokines and subsequently reduced chemoreceptor activity.

A somewhat conflicting finding in our study was the lack of efficacy of MnTE-2-PyP^{5+} on macrophage activation in the very early (2 h and 6 h) treatment groups. This was in contrast to significantly decreased numbers of activated macrophages in the 12 h and 8 w groups. This lack of effect of MnTE-2-PyP^{5+} on macrophage activation in early treatment time points has been seen in a former study in which the first injection of MnTE-2-PyP^{5+} (6 mg/kg) was started 2 hours after IR and was continued for 2 weeks [10]. In another study, the chronological sequence of macrophage activation after IR was investigated [1]. It was noted that infiltration of activated macrophages into the rat lung started 4 weeks after IR. The number of macrophages rose until the tenth week before it started to decline. At present, there is no sufficient explanation for the observed treatment effect in the 12 h group. Nevertheless, at 8 weeks after IR, macrophages are activated and contribute to the chronic inflammation [1]. For the 8 weeks group, we therefore propose that this inflammatory process is disrupted by MnTE-2-PyP^{5+}. Evidence comes from an in-vitro-study, in which MnTE-2-PyP^{5+} proved effective in decreasing $O_2^{\bullet -}$ production by alveolar macrophages with direct consequence for macrophage derived production of VEGF and TGF-β [79].

8-OHdG was increased in almost every irradiated group with a trend towards higher levels of DNA oxidation at later treatment time-points and was significantly elevated in animals being treated 72 h after irradiation or later (8 w). This reflects the ongoing process of oxidation of critical biological molecules. 8-OHdG can be detected as long as cell turnover has not abolished 8-OHdG residues from the DNA compartment. Therefore increased DNA oxidation could be detected as well in the 8w-group despite prominent treatment effects of MnTE-2-PyP^{5+}.

Oxidation/nitrosation of key molecules at physiological levels participates in intracellular signaling processes [3, 55]. However, perpetual elevation of oxidation/nitration/nitrosation -

chronic oxidative/nitrosative stress - is a hallmark of normal tissue radiogenic injury [1, 2, 7, 17, 27]. It is unclear, whether therapeutics like MnTE-2-PyP^{5+} only suppress this elevated state or even terminally reconstitute the steady state in physiological redox signaling. In this respect, the optimal length of treatment has to be evaluated. Our group recently showed that treatment with MnPs for the duration of ten weeks after radiation, but not for only one week, is able to robustly suppress radiation-induced lung inflammation [11]. Future studies should address two main issues: (1) would treatment provide beneficial effects long after the cessation of therapy; and (2) would treatment longer than 2 weeks be necessary for the best outcome of radiation-induced lung damage.

Furthermore, additional toxicity studies are necessary. In respect to acute toxicity in our model, subcutaneous (s.c.) implantation of osmotic pumps was better tolerated than s.c. injections as done in a previous study [10]. Furthermore, continuous application of MnTE-2-PyP^{5+} is preferable to single s.c. daily injections due to the compound's half-life in plasma of 60 min [80].

With respect to the possible use of MnP in protecting normal tissue during tumor radiotherapy, it is important to note that MnTE-2-PyP^{5+} will not protect tumors against radiation. While it is not toxic to tumor cells in its own right [8, 81, 82], MnTE-2-PyP^{5+} suppresses tumor growth *via* anti-angiogenic effects at the level of tumor vasculature [83]. Thus, by suppressing tumor oxidative stress which in turn suppresses redox-based activation of HIF-1α and downstream VEGF, angiogenesis is downregulated [83]. Moreover in combination with radiation [81] and chemotherapy [84], MnTE-2-PyP^{5+} enhanced tumor growth suppression was observed.

In conclusion, the current results provide further evidence that MnTE-2-PyP^{5+} is effective in ameliorating and treating radiation-induced lung injury presumably *via* scavenging signaling reactive species and therefore suppressing excessive upregulation of inflammatory and immune pathways. In the past, we have shown that preemptive or early treatment after radiation can effectively reverse activation of transcription factors (HIF-1α, NF-κB), reduce hypoxia (CA-IX positive staining), prevent activation of alveolar macrophages (ED-1), decrease activation of latent TGF-β and production of VEGF, and subsequently prevent higher degree of histopathological (H&E and Masson's Trichrome staining) and functional lung damage (breathing frequencies) [10-14]. Our results presented now suggest that there is a crucial temporal time span in which early therapy of radiation-induced lung injury with antioxidants should be initiated. Nevertheless, late (rescue) treatment might become an option if early therapy is not achievable.

Acknowledgments

This study was supported in part by the National Institutes of Health (Grant numbers NIH-U19-AI-067798 and RO1 CA 098452 for Z.V.)

Literature

1. Fleckenstein K, Zgonjanin L, Chen L, Rabbani Z, Jackson IL, Thrasher B, Kirkpatrick J, Foster WM, Vujaskovic Z. Temporal onset of hypoxia and oxidative stress after pulmonary irradiation. Int J Radiat Oncol Biol Phys. 2007; 68:196–204. [PubMed: 17448873]
2. Vujaskovic Z, Anscher MS, Feng QF, Rabbani ZN, Amin K, Samulski TS, Dewhirst MW, Haroon ZA. Radiation-induced hypoxia may perpetuate late normal tissue injury. Int J Radiat Oncol Biol Phys. 2001; 50:851–855. [PubMed: 11429211]
3. Mikkelsen RB, Wardman P. Biological chemistry of reactive oxygen and nitrogen and radiation-induced signal transduction mechanisms. Oncogene. 2003; 22:5734–5754. [PubMed: 12947383]

4. Leach JK, Van Tuyle G, Lin PS, Schmidt-Ullrich R, Mikkelsen RB. Ionizing radiation-induced, mitochondria-dependent generation of reactive oxygen/nitrogen. Cancer Res. 2001; 61:3894–3901. [PubMed: 11358802]
5. Pearce LL, Epperly MW, Greenberger JS, Pitt BR, Peterson J. Identification of respiratory complexes I and III as mitochondrial sites of damage following exposure to ionizing radiation and nitric oxide. Nitric Oxide. 2001; 5:128–136. [PubMed: 11292362]
6. Zorov DB, Filburn CR, Klotz LO, Zweier JL, Sollott SJ. Reactive oxygen species (ROS)-induced ROS release: a new phenomenon accompanying induction of the mitochondrial permeability transition in cardiac myocytes. J Exp Med. 2000; 192:1001–1014. [PubMed: 11015441]
7. Li F, Sonveaux P, Rabbani ZN, Liu S, Yan B, Huang Q, Vujaskovic Z, Dewhirst MW, Li CY. Regulation of HIF-1alpha stability through S-nitrosylation. Mol Cell. 2007; 26:63–74. [PubMed: 17434127]
8. Moeller BJ, Cao Y, Li CY, Dewhirst MW. Radiation activates HIF-1 to regulate vascular radiosensitivity in tumors: role of reoxygenation, free radicals, and stress granules. Cancer Cell. 2004; 5:429–441. [PubMed: 15144951]
9. Tse HM, Milton MJ, Piganelli JD. Mechanistic analysis of the immunomodulatory effects of a catalytic antioxidant on antigen-presenting cells: implication for their use in targeting oxidation-reduction reactions in innate immunity. Free Radic Biol Med. 2004; 36:233–247. [PubMed: 14744635]
10. Gauter-Fleckenstein B, Fleckenstein K, Owzar K, Jiang C, Batinic-Haberle I, Vujaskovic Z. Comparison of two Mn porphyrin-based mimics of superoxide dismutase in pulmonary radioprotection. Free Radic Biol Med. 2008; 44:982–989. [PubMed: 18082148]
11. Rabbani ZN, Batinic-Haberle I, Anscher MS, Huang J, Day BJ, Alexander E, Dewhirst MW, Vujaskovic Z. Long-term administration of a small molecular weight catalytic metalloporphyrin antioxidant, AEOL 10150, protects lungs from radiation-induced injury. Int J Radiat Oncol Biol Phys. 2007; 67:573–580. [PubMed: 17236973]
12. Rabbani ZN, Salahuddin FK, Yarmolenko P, Batinic-Haberle I, Thrasher BA, Gauter-Fleckenstein B, Dewhirst MW, Anscher MS, Vujaskovic Z. Low molecular weight catalytic metalloporphyrin antioxidant AEOL 10150 protects lungs from fractionated radiation. Free Radic Res. 2007; 41:1273–1282. [PubMed: 17957541]
13. Vujaskovic Z, Batinic-Haberle I, Rabbani ZN, Feng QF, Kang SK, Spasojevic I, Samulski TV, Fridovich I, Dewhirst MW, Anscher MS. A small molecular weight catalytic metalloporphyrin antioxidant with superoxide dismutase (SOD) mimetic properties protects lungs from radiation-induced injury. Free Radic Biol Med. 2002; 33:857–863. [PubMed: 12208373]
14. Vujaskovic Z, Batinic-Haberle I, Rabbani ZN, Spasojevic I, Samulski TV, Fridovich I, Dewhirst MW, Anscher MS. Effects of metalloporphyrin catalytic antioxidant AEOL 10113 on radiation-induced lung injury. Free Radical Biology and Medicine. 2002; 33:S239–S239.
15. Moulder JE, Cohen EP. Future strategies for mitigation and treatment of chronic radiation-induced normal tissue injury. Semin Radiat Oncol. 2007; 17:141–148. [PubMed: 17395044]
16. Zhao W, Diz DI, Robbins ME. Oxidative damage pathways in relation to normal tissue injury. Br J Radiol. 2007; 80 Spec No 1:S23–31. [PubMed: 17704323]
17. Robbins ME, Zhao W. Chronic oxidative stress and radiation-induced late normal tissue injury: a review. Int J Radiat Biol. 2004; 80:251–259. [PubMed: 15204702]
18. Batinic-Haberle I. Manganese porphyrins and related compounds as mimics of superoxide dismutase. Methods Enzymol. 2002; 349:223–233. [PubMed: 11912911]
19. Batinic-Haberle I, Benov L, Spasojevic I, Fridovich I. The ortho effect makes manganese(III) meso-tetrakis(N-methylpyridinium-2-yl)porphyrin a powerful and potentially useful superoxide dismutase mimic. J Biol Chem. 1998; 273:24521–24528. [PubMed: 9733746]
20. Salvemini D, Wang ZQ, Zweier JL, Samouilov A, Macarthur H, Misko TP, Currie MG, Cuzzocrea S, Sikorski JA, Riley DP. A nonpeptidyl mimic of superoxide dismutase with therapeutic activity in rats. Science. 1999; 286:304–306. [PubMed: 10514375]
21. Baker K, Marcus CB, Huffman K, Kruk H, Malfroy B, Doctrow SR. Synthetic combined superoxide dismutase/catalase mimetics are protective as a delayed treatment in a rat stroke model:

a key role for reactive oxygen species in ischemic brain injury. J Pharmacol Exp Ther. 1998; 284:215–221. [PubMed: 9435181]

22. Goldstein S, Samuni A, Hideg K, Merenyi G. Structure-activity relationship of cyclic nitroxides as SOD mimics and scavengers of nitrogen dioxide and carbonate radicals. J Phys Chem A. 2006; 110:3679–3685. [PubMed: 16526651]
23. Batinic-Haberle I, Reboucas J, Spasojevic I. Superoxide dismutase mimics: chemistry, pharmacology and therapeutic potential. Antiox Redox Signal. 2009 in press.
24. Murphy MP. Targeting lipophilic cations to mitochondria. Biochim Biophys Acta. 2008; 1777:1028–1031. [PubMed: 18439417]
25. Munroe W, Kingsley C, Durazo A, Gralla EB, Imlay JA, Srinivasan C, Valentine JS. Only one of a wide assortment of manganese-containing SOD mimicking compounds rescues the slow aerobic growth phenotypes of both Escherichia coli and Saccharomyces cerevisiae strains lacking superoxide dismutase enzymes. J Inorg Biochem. 2007; 101:1875–1882. [PubMed: 17723242]
26. Pollard JM, Reboucas JS, Durazo A, Kos I, Fike F, Panni M, Gralla EB, Valentine JS, Batinic-Haberle I, Gatti RA. Radio-protective effects of manganese-containing superoxide dismutase mimics on ataxia telangiectasia cells. Free Radic Biol Med. 2009
27. Langan AR, Khan MA, Yeung IW, Van Dyk J, Hill RP. Partial volume rat lung irradiation: the protective/mitigating effects of Eukarion-189, a superoxide dismutasecatalase mimetic. Radiother Oncol. 2006; 79:231–238. [PubMed: 16675053]
28. Lee JH, Park JW. A manganese porphyrin complex is a novel radiation protector. Free Radic Biol Med. 2004; 37:272–283. [PubMed: 15203198]
29. Spasojevic I, Chen Y, Noel TJ, Yu Y, Cole MP, Zhang L, Zhao Y, St Clair DK, Batinic-Haberle I. Mn porphyrin-based superoxide dismutase (SOD) mimic, Mn(III)TE-2-PyP(5+), targets mouse heart mitochondria. Free Radic Biol Med. 2007; 42:1193–1200. [PubMed: 17382200]
30. Ferrer-Sueta G, Hannibal L, Batinic-Haberle I, Radi R. Reduction of manganese porphyrins by flavoenzymes and submitochondrial particles: a catalytic cycle for the reduction of peroxynitrite. Free Radic Biol Med. 2006; 41:503–512. [PubMed: 16843831]
31. Ferrer-Sueta G, Vitturi D, Batinic-Haberle I, Fridovich I, Goldstein S, Czapski G, Radi R. Reactions of manganese porphyrins with peroxynitrite and carbonate radical anion. J Biol Chem. 2003; 278:27432–27438. [PubMed: 12700236]
32. Uozaki H, Fukayama M, Nakagawa K, Ishikawa T, Misawa S, Doi M, Maekawa K. The pathology of multi-organ involvement: two autopsy cases from the Tokaimura criticality accident. BJR Suppl. 2005; 27:13–16. [PubMed: 15975865]
33. Baranov AE, Selidovkin GD, Butturini A, Gale RP. Hematopoietic recovery after 10-Gy acute total body radiation. Blood. 1994; 83:596–599. [PubMed: 8286754]
34. Perez CA, Bauer M, Edelstein S, Gillespie BW, Birch R. Impact of tumor control on survival in carcinoma of the lung treated with irradiation. Int J Radiat Oncol Biol Phys. 1986; 12:539–547. [PubMed: 3009368]
35. Perez CA, Stanley K, Rubin P, Kramer S, Brady L, Perez-Tamayo R, Brown GS, Concannon J, Rotman M, Seydel HG. A prospective randomized study of various irradiation doses and fractionation schedules in the treatment of inoperable non-oat-cell carcinoma of the lung. Preliminary report by the Radiation Therapy Oncology Group. Cancer. 1980; 45:2744–2753. [PubMed: 6991092]
36. Saunders M, Dische S, Barrett A, Harvey A, Griffiths G, Palmar M. Continuous, hyperfractionated, accelerated radiotherapy (CHART) versus conventional radiotherapy in non-small cell lung cancer: mature data from the randomised multicentre trial. CHART Steering committee. Radiother Oncol. 1999; 52:137–148. [PubMed: 10577699]
37. Willner J, Baier K, Caragiani E, Tschammler A, Flentje M. Dose, volume, and tumor control prediction in primary radiotherapy of non-small-cell lung cancer. Int J Radiat Oncol Biol Phys. 2002; 52:382–389. [PubMed: 11872283]
38. Wurschmidt F, Bunemann H, Bunemann C, Beck-Bornholdt HP, Heilmann HP. Inoperable non-small cell lung cancer: a retrospective analysis of 427 patients treated with high-dose radiotherapy. Int J Radiat Oncol Biol Phys. 1994; 28:583–588. [PubMed: 8113101]

39. Fleckenstein K, Gauter-Fleckenstein B, Jackson IL, Rabbani Z, Anscher M, Vujaskovic Z. Using biological markers to predict risk of radiation injury. Semin Radiat Oncol. 2007; 17:89–98. [PubMed: 17395039]
40. Batinic-Haberle I, Spasojevic I, Stevens RD, Hambright P, Fridovich I. Manganese(III) meso-tetrakis(ortho-N-alkylpyridyl)porphyrins. Synthesis, characterization, and catalysis of O-2(center dot-) dismutation. J Chem Soc Dalton Trans. 2002:2689–2696.
41. Ashcroft T, Simpson JM, Timbrell V. Simple method of estimating severity of pulmonary fibrosis on a numerical scale. J Clin Pathol. 1988; 41:467–470. [PubMed: 3366935]
42. Hsu SM, Raine L, Fanger H. Use of avidin-biotin-peroxidase complex (ABC) in immunoperoxidase techniques: a comparison between ABC and unlabeled antibody (PAP) procedures. J Histochem Cytochem. 1981; 29:577–580. [PubMed: 6166661]
43. Agresti, A. Categorical data analysis. New York: Wiley; 1990.
44. Hajek, J.; Sidak, Z.; Pranab, K. Theory of Rank Tests. San Diego: Academic Press; 1999.
45. Pinheiro, JCB.; D, M. Mixed-Effects Models in S and S-PLUS. New York: Springer; 2000.
46. Team, R. D. C. R: A language and environment for statistical computing. Vienna, Austria: R Foundation for Statistical Computing; 2007.
47. Fischer-Nielsen A, Jeding IB, Loft S. Radiation-induced formation of 8-hydroxy-2′-deoxyguanosine and its prevention by scavengers. Carcinogenesis. 1994; 15:1609–1612. [PubMed: 8055639]
48. Withers, HR.; Peters, LJ.; Kogelnik, HS. The pathobiology of late effects in irradiation. In: Meyn, RE.; Withers, HR., editors. Radiation biology in cancer research. Vol. 1980. New York: Raven Press; p. 439-448.
49. Bentzen SM. Preventing or reducing late side effects of radiation therapy: radiobiology meets molecular pathology. Nat Rev Cancer. 2006; 6:702–713. [PubMed: 16929324]
50. Trott KR, Herrmann T, Kasper M. Target cells in radiation pneumopathy. Int J Radiat Oncol Biol Phys. 2004; 58:463–469. [PubMed: 14751516]
51. Pena LA, Fuks Z, Kolesnick R. Stress-induced apoptosis and the sphingomyelin pathway. Biochem Pharmacol. 1997; 53:615–621. [PubMed: 9113079]
52. Moosavi H, McDonald S, Rubin P, Cooper R, Stuard ID, Penney D. Early radiation dose-response in lung: an ultrastructural study. Int J Radiat Oncol Biol Phys. 1977; 2:921–931. [PubMed: 591409]
53. Travis EL. The sequence of histological changes in mouse lungs after single doses of x-rays. Int J Radiat Oncol Biol Phys. 1980; 6:345–347. [PubMed: 7390907]
54. Jurmann MJ, Dammenhayn L, Schaefers HJ, Haverich A. Pulmonary reperfusion injury: evidence for oxygen-derived free radical mediated damage and effects of different free radical scavengers. Eur J Cardiothorac Surg. 1990; 4:665–670. [PubMed: 2288747]
55. Trachootham D, Lu W, Ogasawara MA, Nilsa RD, Huang P. Redox regulation of cell survival. Antioxid Redox Signal. 2008; 10:1343–1374. [PubMed: 18522489]
56. Finkelstein JN, Johnston CJ, Baggs R, Rubin P. Early alterations in extracellular matrix and transforming growth factor beta gene expression in mouse lung indicative of late radiation fibrosis. Int J Radiat Oncol Biol Phys. 1994; 28:621–631. [PubMed: 8113105]
57. Johnston CJ, Piedboeuf B, Rubin P, Williams JP, Baggs R, Finkelstein JN. Early and persistent alterations in the expression of interleukin-1 alpha, interleukin-1 beta and tumor necrosis factor alpha mRNA levels in fibrosis-resistant and sensitive mice after thoracic irradiation. Radiat Res. 1996; 145:762–767. [PubMed: 8643837]
58. Robbins ME, Diz DI. Pathogenic role of the renin-angiotensin system in modulating radiation-induced late effects. Int J Radiat Oncol Biol Phys. 2006; 64:6–12. [PubMed: 16377409]
59. Rubin P, Johnston CJ, Williams JP, McDonald S, Finkelstein JN. A perpetual cascade of cytokines postirradiation leads to pulmonary fibrosis. Int J Radiat Oncol Biol Phys. 1995; 33:99–109. [PubMed: 7642437]
60. Greenberger JS. Radioprotection. In Vivo. 2009; 23:323–336. [PubMed: 19414422]
61. Zhao W, Robbins ME. Inflammation and chronic oxidative stress in radiation-induced late normal tissue injury: therapeutic implications. Curr Med Chem. 2009; 16:130–143. [PubMed: 19149566]

62. Cohen EP, Fish BL, Moulder JE. Successful brief captopril treatment in experimental radiation nephropathy. J Lab Clin Med. 1997; 129:536–547. [PubMed: 9142050]
63. Molteni A, Moulder JE, Cohen EF, Ward WF, Fish BL, Taylor JM, Wolfe LF, Brizio-Molteni L, Veno P. Control of radiation-induced pneumopathy and lung fibrosis by angiotensin-converting enzyme inhibitors and an angiotensin II type 1 receptor blocker. Int J Radiat Biol. 2000; 76:523–532. [PubMed: 10815633]
64. Ward WF, Kim YT, Molteni A, Solliday NH. Radiation-induced pulmonary endothelial dysfunction in rats: modification by an inhibitor of angiotensin converting enzyme. Int J Radiat Oncol Biol Phys. 1988; 15:135–140. [PubMed: 3292488]
65. Ward WF, Molteni A, Ts'ao CH, Hinz JM. Captopril reduces collagen and mast cell accumulation in irradiated rat lung. Int J Radiat Oncol Biol Phys. 1990; 19:1405–1409. [PubMed: 2262365]
66. Ward WF, Molteni A, Ts'ao CH, Kim YT, Hinz JM. Radiation pneumotoxicity in rats: modification by inhibitors of angiotensin converting enzyme. Int J Radiat Oncol Biol Phys. 1992; 22:623–625. [PubMed: 1735701]
67. Delanian S, Porcher R, Rudant J, Lefaix JL. Kinetics of response to long-term treatment combining pentoxifylline and tocopherol in patients with superficial radiation-induced fibrosis. J Clin Oncol. 2005; 23:8570–8579. [PubMed: 16260695]
68. Brush J, Lipnick SL, Phillips T, Sitko J, McDonald JT, McBride WH. Molecular mechanisms of late normal tissue injury. Semin Radiat Oncol. 2007; 17:121–130. [PubMed: 17395042]
69. Denham JW, Hauer-Jensen M. The radiotherapeutic injury--a complex 'wound'. Radiother Oncol. 2002; 63:129–145. [PubMed: 12063002]
70. Cragg PA, Drysdale DB. Interaction of hypoxia and hypercapnia on ventilation, tidal volume and respiratory frequency in the anaesthetized rat. J Physiol. 1983; 341:477–493. [PubMed: 6413681]
71. James PE, Grinberg OY, Swartz HM. Superoxide production by phagocytosing macrophages in relation to the intracellular distribution of oxygen. J Leukoc Biol. 1998; 64:78–84. [PubMed: 9665279]
72. Vlessis AA, Bartos D, Muller P, Trunkey DD. Role of reactive O2 in phagocyte-induced hypermetabolism and pulmonary injury. J Appl Physiol. 1995; 78:112–116. [PubMed: 7713799]
73. Jacono FJ, Peng YJ, Nethery D, Faress JA, Lee Z, Kern JA, Prabhakar NR. Acute lung injury augments hypoxic ventilatory response in the absence of systemic hypoxemia. J Appl Physiol. 2006; 101:1795–1802. [PubMed: 16888052]
74. Wang X, Wang BR, Duan XL, Zhang P, Ding YQ, Jia Y, Jiao XY, Ju G. Strong expression of interleukin-1 receptor type I in the rat carotid body. J Histochem Cytochem. 2002; 50:1677–1684. [PubMed: 12486091]
75. Wang X, Zhang XJ, Xu Z, Li X, Li GL, Ju G, Wang BR. Morphological evidence for existence of IL-6 receptor alpha in the glomus cells of rat carotid body. Anat Rec A Discov Mol Cell Evol Biol. 2006; 288:292–296. [PubMed: 16463381]
76. Agapito MT, Sanz-Alfayate G, Gomez-Nino A, Gonzalez C, Obeso A. General redox environment and carotid body chemoreceptor function. Am J Physiol Cell Physiol. 2009; 296:C620–631. [PubMed: 19144860]
77. Csont T, Viappiani S, Sawicka J, Slee S, Altarejos JY, Batinic-Haberle I, Schulz R. The involvement of superoxide and iNOS-derived NO in cardiac dysfunction induced by pro-inflammatory cytokines. J Mol Cell Cardiol. 2005; 39:833–840. [PubMed: 16171809]
78. Piganelli JD, Flores SC, Cruz C, Koepp J, Batinic-Haberle I, Crapo J, Day B, Kachadourian R, Young R, Bradley B, Haskins K. A metalloporphyrin-based superoxide dismutase mimic inhibits adoptive transfer of autoimmune diabetes by a diabetogenic T-cell clone. Diabetes. 2002; 51:347–355. [PubMed: 11812741]
79. Jackson IL, Chen L, Batinic-Haberle I, Vujaskovic Z. Superoxide dismutase mimetic reduces hypoxia-induced O2*-, TGF-beta, and VEGF production by macrophages. Free Radic Res. 2007; 41:8–14. [PubMed: 17164174]
80. Spasojevic I, Chen Y, Noel TJ, Fan P, Zhang L, Reboucas JS, St Clair DK, Batinic-Haberle I. Pharmacokinetics of the potent redox-modulating manganese porphyrin, MnTE-2-PyP(5+), in plasma and major organs of B6C3F1 mice. Free Radic Biol Med. 2008; 45:943–949. [PubMed: 18598757]

81. Moeller BJ, Batinic-Haberle I, Spasojevic I, Rabbani ZN, Anscher MS, Vujaskovic Z, Dewhirst MW. A manganese porphyrin superoxide dismutase mimetic enhances tumor radioresponsiveness. Int J Radiat Oncol Biol Phys. 2005; 63:545–552. [PubMed: 16168847]

82. Ye X, Fels D, Dedeugd C, Dewhirst MW, Leong K, Batinic-Haberle I. The in vitro cytotoxic effects of Mn(III) alkylpyridylporphyrin/ascorbate system on four tumor cell lines. Free Radical Biology and Medicine. 2009; 47 S1:136–158.

83. Rabbani ZN, Spasojevic I, Zhang X, Moeller BJ, Haberle S, Vasquez-Vivar J, Dewhirst MW, Vujaskovic Z, Batinic-Haberle I. Antiangiogenic action of redox-modulating Mn(III) meso-tetrakis(N-ethylpyridinium-2-yl)porphyrin, MnTE-2-PyP(5+), via suppression of oxidative stress in a mouse model of breast tumor. Free Radic Biol Med. 2009; 47:992–1004. [PubMed: 19591920]

84. Jaramillo MC, Frye JB, Crapo JD, Briehl MM, Tome ME. Increased manganese superoxide dismutase expression or treatment with manganese porphyrin potentiates dexamethasone-induced apoptosis in lymphoma cells. Cancer Res. 2009; 69:5450–5457. [PubMed: 19549914]

List of abbreviations

IR	Irradiation
***N*-ethylpyridinium-2-yl) porphyrin (MnTE-2-PyP^{5+}**	Manganese (III) tetrakis
$CO_3^{\bullet-}$	Carbonate radical
$HO^{\bullet}$	Hydroxyl radical
$O_2^{\bullet-}$	Superoxide
$ONOO^-$	Peroxynitrite
HOCl	Hypochlorous acid
H_2O_2	Hydrogen peroxide
H&E	Hematoxylin and eosin
8-OHdG	8-hydroxy-2′ -deoxyguanosine
TGF-β	Transforming growth factor-beta
HIF-1α	Hypoxia inducible factor 1α
VEGF (A)	Vascular endothelial growth factor A
w	weeks
h	hours

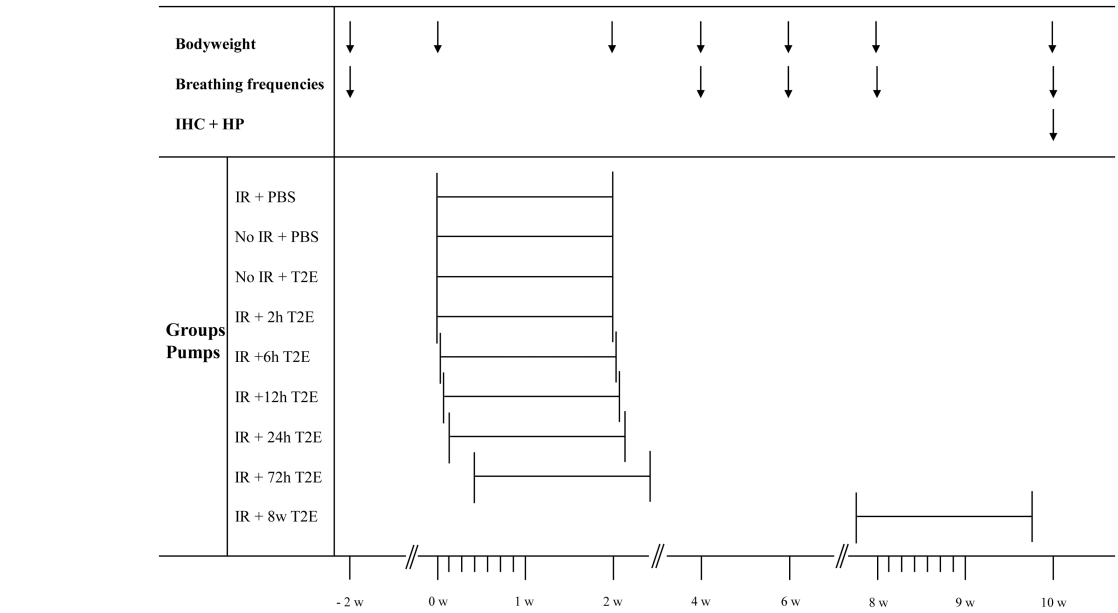

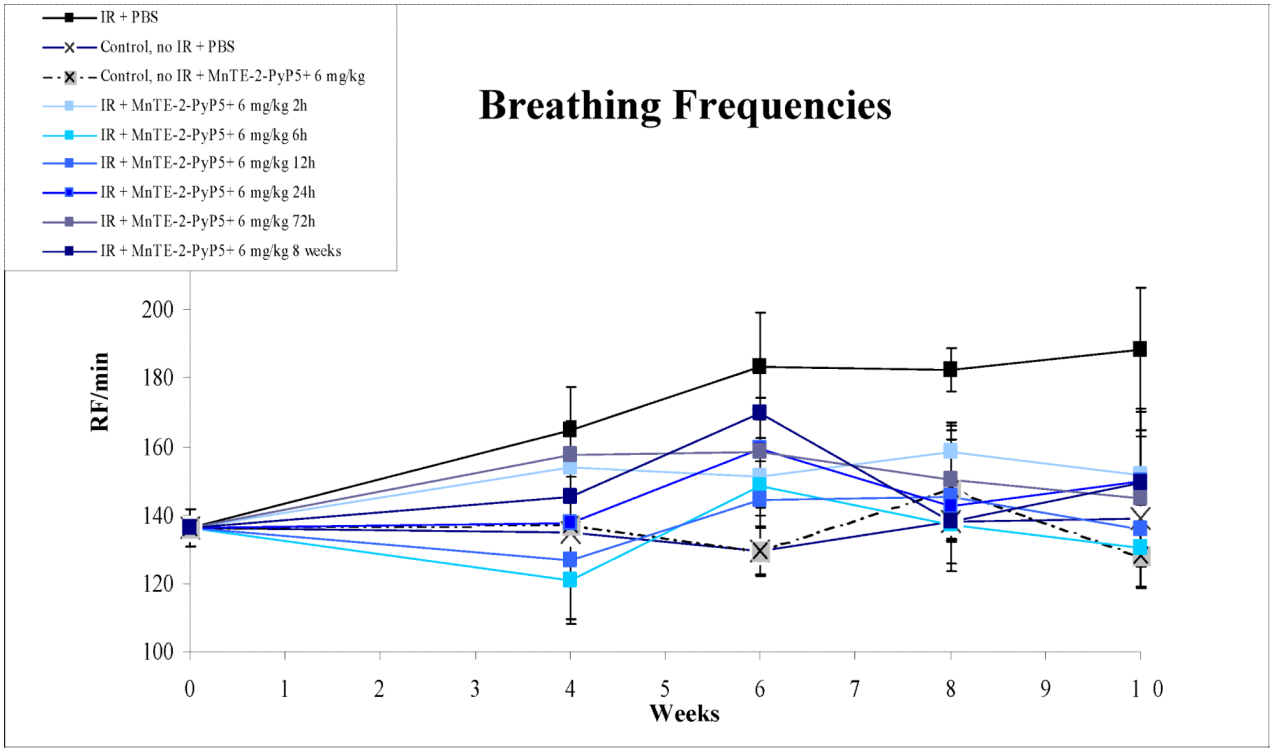

Figure 1.

Breathing frequencies, as recorded bi-weekly from week zero (pre-IR) to week ten (time-point of sacrifice). In comparison to nonirradiated control animals, significantly higher breathing rates were measured in animals which received no treatment after IR (P = 0.0079). Animals, which were irradiated and received MnTE-2-PyP^{5+} post-IR displayed significantly lower breathing rates in comparison to the IR-only group. Animals, which received late treatment starting 8 weeks post-IR displayed a trend towards elevated breathing frequencies

which was not more seen 5 days after starting of treatment (implantation of pumps at day 5 of week 7; measurement of breathing frequencies five days later at day 3 of week 8).

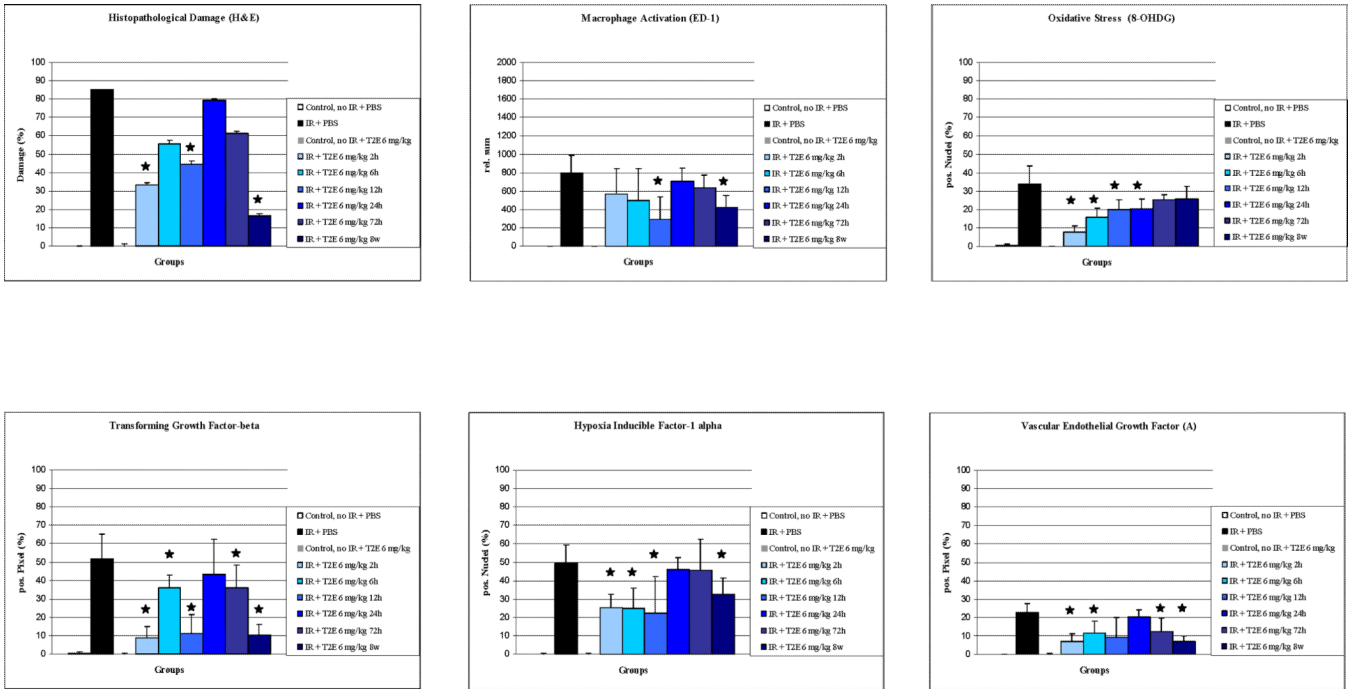

Figure 2.

Comparison of experimental groups on histopathological damage, macrophage activation (ED-1), oxidative stress (8-OHdG), transforming growth factor-β (TGF-β), hypoxia inducible factor-1α (HIF-1α), and vascular endothelial growth factor (A) (VEGF(A)). Results are displayed as vertical bar plots with standard deviation. Asterixes indicate statistical significant differences between IR-only group and IR + MnP treatment groups ($p < 0.05$).

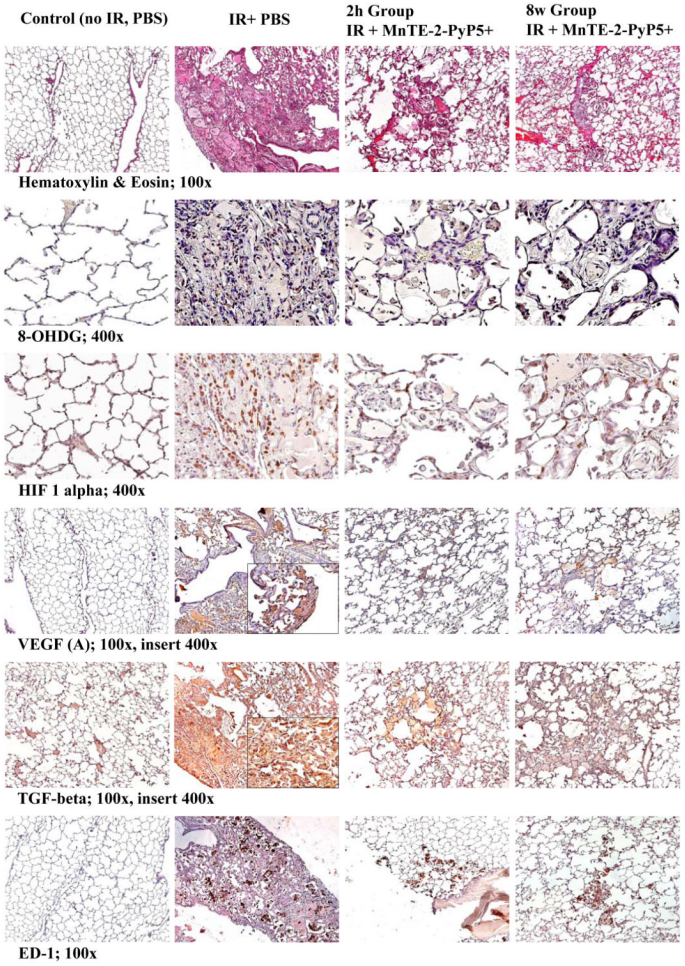

Figure 3.

Representative images of histotpathology (H&E staining) and Immunohistchemistry (8-OhDG, HIF-1α, VEGF (A), TGF-β, ED-1) studies. Magnification 100× for H&E, TGF-ß, VEGF(A), ED-1, Magnification 400× for 8-OHdG and HIF-1α. Groups: Control (no IR + PBS), IR + PBS (TGF-ß and HIF-1α images with 400× insert), IR + MnTE-2-PyP^{5+} (6 mg/kg) 2h group, IR + MnTE-2-PyP^{5+} 8 weeks group. Negative control shows normal lung structure, no positive (brown) immunostaining. IR + PBS shows large area of alveolar edema and cell infiltrates with beginning formation of fibrous masses and prominent immunostaining as well as activated macrophages (brown, localized interstitial and intra-alveolar). IR + MnTE-2-PyP^{5+} (2 h and 8 weeks groups) depict focal localized damage with thickening of alveolar wall, interstitial edema, diminished immunostaining and localized activated macrophages.

Table 1

P-values of tested parameters in histopathology (*HP*), immunhistochemistry (*IHC*) studies, body weight, and breathing frequencies.

	Endpoint	*Stat. Test*	No IR, PBS	No IR, T2E	IR, T2E 2h	IR, T2E 6h	IR, T2E 12h	IR, T2E 24h	IR, T2E 72h	IR, T2E 8w
HP	**H & E**	RST	***0.002***	***0.002***	***0.026***	0.169	***0.039***	0.455	0.225	***0.015***
	H & E	Fisher	***0.002***	***0.002***	0.061	0.455	0.182	1.000	0.455	***0.015***
IHC	**ED-1**	RST	***0.002***	***0.002***	0.179	0.179	***0.004***	0.485	0.179	***0.004***
	8-OHDG	RST	***0.002***	***0.002***	***0.002***	***0.002***	***0.017***	***0.015***	0.093	0.179
	TGF-β	RST	***0.002***	***0.002***	***0.002***	***0.041***	***0.002***	0.309	***0.041***	***0.002***
	HIF-1α	RST	***0.002***	***0.002***	***0.002***	***0.004***	***0.041***	0.699	0.937	***0.015***
	VEGF (A)	RST	***0.002***	***0.002***	***0.002***	***0.015***	0.082	0.309	***0.026***	***0.008***
Weight		RST	***0.012***	***0.005***	0.129	0.149	***0.031***	0.096	0.137	0.758
Resp. Rate		RST	***0.008***	***0.008***	***0.008***	***0.008***	***0.008***	***0.008***	***0.016***	***0.008***

Group comparison vs. IR + PBS group. P-values were determined by Wilcoxon rank sum test (RST) and Fisher's test (Fisher) for binomial values; p –value < 0.05 is considered significant.

HP: Hematoxylin & Eosin (H&E; structural damage). *IHC*: 8-hydroxydiguanosine (8-OHDG; DNA-oxidation), transforming growth factor-beta (TGF-β; key factor in development of lung fibrosis), hypoxia inducible factor-1 alpha (HIF-1α; alpha subunit of the transcription factor responsible for VEGF), vascular endothelial growth factor (A) (VEGF (A); growth factor responsible for angiogenesis and endothelial leakage, regulated by HIF-1), ED-1 (ED-1 antibody for CD 68 antigen in activated rat macrophages).

Weight/ Resp. Rate (Breathing Frequencies): P-values for pairwise (IR + PBS vs. control/treatment groups) comparison of distributions of area under the curve as measure of the entire time-course of ten weeks post-IR.